Journal of Technology Research (JTR)
Volume 3, Special Issue, (2025), pp 684-702 ISSN 3005-639X
The 7th Conference of Engineering Sciences and Technology
(CEST-2025)

# Effect of Graphite Content on the Physical and Mechanical Properties of Self-Lubricating Iron-Based Composites Fabricated by Powder Metallurgy

Mohamed A. Ballem*[1], Mohamed O. Sari[1]

[1]Department of Materials Science and Engineering, Faculty of Engineering, Misurata University, Misurata, Libya.

*Corresponding author email: mohamed.ballem@eng.misuratau.edu.ly

Received: 14-10-2025| Accepted: 02-11-2025| Available online:25-12-2025 | DOI:10.26629/jtr.2025.64

## ABSTRACT

This study investigated the physical and mechanical properties of a self-lubricating iron-based material reinforced with different weight percentages of graphite. The specimens were prepared using the powder metallurgy technique by designing and fabricating a suitable die for compacting sponge iron powders containing graphite in weight ratios ranging from 0% to 20%, followed by sintering at 1200 °C. The prepared samples were subjected to several laboratory tests, including green strength, green and sintered density, porosity, dimensional changes, hardness, compressive strength, and abrasive wear, to evaluate the effect of graphite content on the physical and mechanical properties. Microscopic examination was also carried out to track microstructural changes and relate them to the obtained results. The findings showed a decrease in porosity and an increase in density after sintering, accompanied by a 24% improvement in hardness. In the abrasive wear test, the addition of graphite reduced the average weight loss by about 74%, with the 1 wt% graphite sample exhibiting the best performance. All graphite-containing samples demonstrated improved wear resistance exceeding 340%, reaching a peak of about 570% for the 1 wt% graphite specimen compared with the pure iron sample. However, samples with higher graphite contents (≥ 5 wt%) showed separation of graphite from the iron matrix during sintering. Microscopic analysis confirmed that from 2.5 wt% graphite onwards, the graphite phase increased in size and formed voids within the structure, leading to deterioration of mechanical properties. The study concluded that incorporating 1 wt% graphite provides the optimum composition, offering an effective balance between self-lubrication and mechanical strength, and is therefore suitable for use in self-lubricating bearings and power transmission components.

**Keywords:** Abrasive wear; Composites; Graphite; Powder metallurgy; Self-lubricating materials; Sponge iron.

# تأثير نسبة الجرافيت على الخواص الفيزيائية والميكانيكية لمادة ذاتيّة التَّزييت ذات أساس حديديّ مصنَّعة بتقنية ميتالورجيا المساحيق

محمد علي بلعم*[1]، محمد عمران ساري[1]

[1]قسم هندسة وعلوم المواد، كلية الهندسة، جامعة مصراتة، مصراتة، ليبيا.

## ملخـــــص البحـــــث

تناول هذا البحث دراسةً لمجموعة من الخواص الفيزيائية والميكانيكية لمادة ذاتية التزييت ذات أساس حديدي مدعَّمة بنسب وزنية متفاوتة من الجرافيت. تم تحضير العينات باستخدام تقنية ميتالورجيا المساحيق، وذلك بتصميم وتصنيع قالب كبس مناسب استُعمل لكبس مساحيق الحديد الإسفنجي المحتوية على الجرافيت بنسب وزنية من 0% إلى 20%، وأُجريت عملية التلبيد عند 1200 درجة مئوية. أُخضعت العينات لمجموعة من الاختبارات المعملية شملت: المقاومة الخضراء، الكثافة والمسامية قبل وبعد التلبيد، التغير في الأبعاد، الصلادة، مقاومة الضغط، والبلى الاحتكاكي، وذلك لدراسة تأثير محتوى الجرافيت على الخواص الفيزيائية والميكانيكية. أُجري الفحص المجهري لتتبع التغيرات المجهرية وربطها بالنتائج. أظهرت النتائج انخفاضًا في المسامية وزيادة في الكثافة بعد التلبيد، إلى جانب تحسن في الصلادة بنسبة تقارب 24%. في اختبار البلى الاحتكاكي، ساهمت إضافة الجرافيت في تقليل الفقد في الوزن بنسبة متوسطة بلغت نحو 74%، وسجّلت العينة المحتوية على 1% جرافيت أفضل أداء. أيضاً أظهرت جميع العينات الحاوية على الجرافيت تحسنًا في مقاومة البلى بنسبة تجاوزت 340%، وبلغ هذا التحسن ذروته في العينة 1% جرافيت، التي سجلت زيادة تقدّر بحوالي 570% مقارنة بالعينة الخالية من الجرافيت؛ أما العينات ذات النسب العالية من الجرافيت (5% فأكثر)، فقد أبدت انفصالًا للجرافيت عن المصفوفة الحديدية أثناء التلبيد. أكّد الفحص المجهري أنه ابتداءً من 2.5% جرافيت، يزداد حجم الجرافيت في بنية المادة مع احتوائه على فراغات، مما يفسّر بداية تدهور الخواص الميكانيكية. خلصت الدراسة إلى أن 1% جرافيت تمثل النسبة المثلى التي توازن بين التزييت وتحسن الخواص الميكانيكية، مما يُتيح تصنيع مركبات مساحيق عملية تناسب المحامل ذاتية التزييت وأجزاء نقل الحركة وغيرها من التطبيقات المتقدمة في هندسة وعلوم المواد.

**الكلمات الدالة:** البلى الاحتكاكي ؛الجرافيت؛ الحديد الإسفنجي؛ المواد ذاتية التزييت؛ المواد المركبة؛ ميتالورجيا المساحيق.

## INTRODUCTION

Powder metallurgy (PM) is a well-established manufacturing technique widely used to produce metallic components by compacting metal powders followed by sintering at elevated temperatures. This method provides significant advantages, including near-net-shape production, minimal machining waste, precise control of composition and porosity, and the ability to combine dissimilar materials to form engineered composites [1-3]. During sintering, atomic diffusion promotes bonding between particles, decreases porosity, and enhances mechanical integrity [4, 5]. Because of these benefits, PM has become a preferred technique in automotive, aerospace, and tooling industries where component reliability and material efficiency are critical.

Self-lubricating materials constitute a special class of PM products designed for service where external lubrication is difficult or impractical, such as in bearings, sliding interfaces, or vacuum and high-temperature environments. These materials contain a solid-lubricant phase dispersed within a metallic matrix. When friction occurs, the lubricant forms a thin film on the contact surface, reducing wear and friction. Common lubricants include graphite, molybdenum disulfide ($MoS_2$), and boron nitride [6, 7]. Among them, graphite is particularly attractive due to its lamellar crystal structure, excellent thermal stability, and chemical inertness. However, because graphite is softer than iron, its amount must be optimized to achieve effective lubrication without compromising strength or cohesion of the matrix.

Previous studies have investigated the influence of graphite content and processing parameters on the mechanical and tribological behavior of iron-based powder metallurgy composites. Sanyal et al. [8] examined Fe + C preforms and reported that 2 wt% graphite at 1050 °C produced superior wear resistance. Similarly,

Zhang et al. [9] found that increasing graphite content improved density and hardness up to an optimum level before leading to degradation at higher concentrations. De Lima et al. [10] analyzed Fe–$MoS_2$ self-lubricating composites and demonstrated that careful control of the solid-state reaction during sintering significantly enhanced tribological performance by stabilizing the lubricant phase within the iron matrix.

Complementary work by Xiao et al. [11] established quantitative relationships among lubricant content, lubricating-film coverage, and friction coefficient in metal-matrix self-lubricating composites, providing valuable insight into the mechanisms of film formation and friction control. Ye et al. [12] presented an extensive overview of recent advances in self-lubricating metal matrix nanocomposites reinforced by carbonaceous materials, highlighting the critical influence of graphite morphology, dispersion uniformity, and interfacial bonding on achieving an optimal balance between strength and lubrication. In a related study, Moghadam et al. [13] demonstrated that carbon-based reinforcements such as graphene and carbon nanotubes markedly improve wear resistance and mechanical stability through combined solid-lubrication and load-transfer mechanisms. More recently, Araya et al. [14] investigated the morpho-dimensional evolution of solid-lubricant reservoirs in sintered iron-based composites and revealed that geometric transformation of graphite-rich regions during service directly affects long-term wear resistance.

Despite these advances, most existing studies have been restricted to narrow graphite content ranges (typically up to 2–5 wt%) and have focused on a limited set of parameters such as hardness or friction coefficient. However, comprehensive investigations that correlate a broad range of physical and mechanical properties such as density, porosity, dimensional stability, hardness, compressive strength, and abrasive-wear resistance remain scarce. Moreover, the critical threshold beyond which graphite addition compromises matrix cohesion through void formation or phase separation has not been clearly established. These research gaps underscore the need for a systematic evaluation across an extended range of graphite contents.

The objective of this study is therefore to investigate the influence of graphite content (0–20 wt%) on the physical and mechanical behavior of self-lubricating iron-based composites produced by powder metallurgy. By extending the graphite range beyond conventional limits, this research aims to determine the optimal graphite fraction that balances lubrication and strength while clarifying the mechanism of performance degradation at higher contents. Detailed experimental evaluations including density, porosity, hardness, compressive strength, and abrasive-wear resistance are complemented by microscopic observations that elucidate the mechanisms of lubrication, microstructural evolution, and void development.

The present work contributes to the field by providing an integrated understanding of the relationships between graphite content, microstructure, and overall performance of iron–graphite composites across a broader compositional spectrum than previously reported. The findings offer practical guidance for designing durable self-lubricating components for advanced engineering applications where maintenance-free operation and extended service life are required.

## 2. MATERIALS AND METHODS

### *2.1. Materials*

The raw materials used in this study were obtained from the Libyan Iron and Steel Company (LISCO), Misurata, Libya. The base material was sponge iron powder (direct-reduced iron, DRI) supplied in fine powder form, as shown in Figure 1(a). Its chemical composition is listed in Table 1. Graphite, with

a carbon purity exceeding 99% and ash content below 0.2%, was supplied in solid pieces of approximately 10–15 cm, later ground and sieved to the required particle size, as shown in Figure 1(b). Anthracite was not included in the sample compositions; it was used only as a protective medium during sintering to minimize oxidation. The anthracite granules, ranging in size from 2 to 6 mm, are shown in Figure 1(c), and their main characteristics are summarized in Table 2.

**Table 1.** Chemical composition of sponge iron.

| Component | (%wt) |
|---|---|
| **Fe Total** | %91 – %93 |
| **Fe Metallic** | %83 – %88 |
| **$SiO_2$** | %2.0 – %3.5 |
| **$Al_2O_3$** | %0.5 – %1.5 |
| **CaO** | %0.3 – %2.5 |
| **C** | %1.3 – %2.5 |
| **P** | %0.02 – %0.04 |
| **S** | %0.005 – %0.15 |

**Table 2.** Main characteristics of anthracite.

| Component | (%wt) |
|---|---|
| **C** | %88 (min) |
| **Ash** | %7.0 (max) |
| **Moisture** | %3 (max) |
| **Volatile** | %1.0 |
| | |

(a)

(b) (c)

**Fig 1.** Raw materials used in specimen preparation: (a) sponge iron, (b) graphite, and (c) anthracite.

### *2.2. Design and Fabrication of Compaction Die*

A custom die set was designed and fabricated to produce cylindrical powder metallurgy specimens. The design, developed using SolidWorks software, is illustrated in Figure 2. Considering the 20 kN capacity of the GUNT WP 300 press, the die diameter was set to 10 mm, corresponding to a compaction pressure of about 250 MPa, adequate for achieving sufficient green strength and dimensional stability.

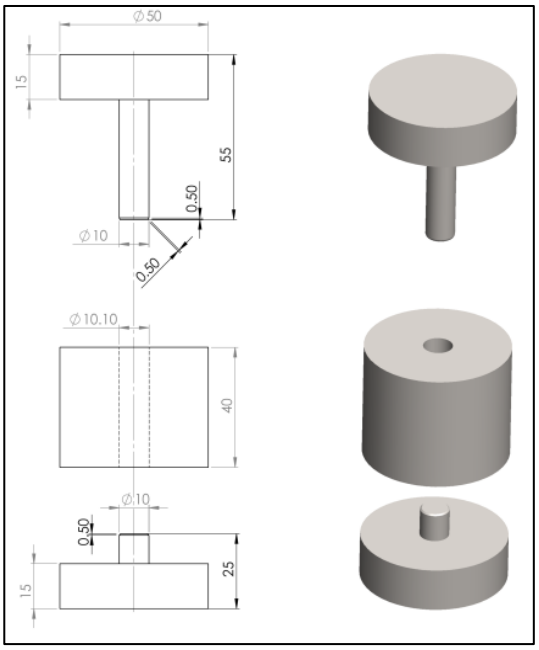


**Fig 2.** Schematic drawing and 3D model of the compaction die prepared using SolidWorks software.

Gray cast iron was selected for die fabrication owing to its adequate compressive strength, ease of machining; its chemical composition is listed in Table 3. Prior to and after machining, the material underwent stress-relieving heat treatments (600 °C for 2 h, followed by furnace cooling) to minimize residual stresses. Machining operations such as facing, turning, and drilling were then performed to produce the final die components, as illustrated in Figure 3. The detailed design calculations and manufacturing procedures are available elsewhere [15].

**Table 3.** Chemical composition (wt%) of the gray cast iron used for die fabrication.

| Element | wt% |
|---|---|
| **C** | 3.826 |
| **Si** | 2.647 |
| **Mn** | 0.64 |
| **P** | 0.037 |
| **S** | 0.11 |
| **Cr** | 0.105 |
| **Mo** | 0.015 |
| **Ni** | 0.09 |
| **Cu** | 0.199 |
| **Sn** | 0.014 |
| **Al** | 0.006 |
| **Co** | 0.011 |
| **Nb** | 0.004 |
| **Ti** | 0.02 |
| **V** | 0.013 |
| **Fe** | Bal. |

**Fig 3.** Photograph of the machined compaction die with the ejector piece (left) used to remove the compacted specimens.

### *2.3. Samples Preparation*

The preparation of specimens followed the conventional stages of powder metallurgy, including powder conditioning, mixing, compaction, and sintering.

In the first stage, sponge iron, graphite, and anthracite powders were oven-dried at 150 °C to remove residual moisture. Graphite pieces were manually crushed prior to milling to facilitate particle size reduction. The required quantities of sponge iron and graphite were then accurately weighed using a precision balance (METTLER TOLEDO Jewelry Carat Balance, model JB1603-L-C; readability 0.1 mg). Powder mixtures containing 0–20 wt% graphite were prepared by manual blending in sealed glass containers for 20 min to ensure uniform distribution.

Compaction was carried out using a universal testing machine (GUNT WP 300, Germany) (Figure 4(a)) at the maximum load capacity of 20 kN, corresponding to an applied pressure of approximately 250 MPa. Each compact was held under load for 1 min to ensure dimensional stability. The resulting cylindrical green specimens (10 mm in diameter × ≈ 10 mm in height) are shown in Figure 4(b). The estimated green densities and calculated masses for each composition were determined using the rule of mixtures, as detailed elsewhere [15].

Sintering was performed in a CARBOLITE RHF 1500 electric furnace (UK) at 1200 °C for 30 min with a constant heating rate of 3 °C/min. To prevent oxidation, each compact was placed inside an individual ceramic crucible filled and fully covered with anthracite powder (Figure 5). The specimens were then allowed to cool gradually inside the furnace to avoid cracking and preserve structural integrity.

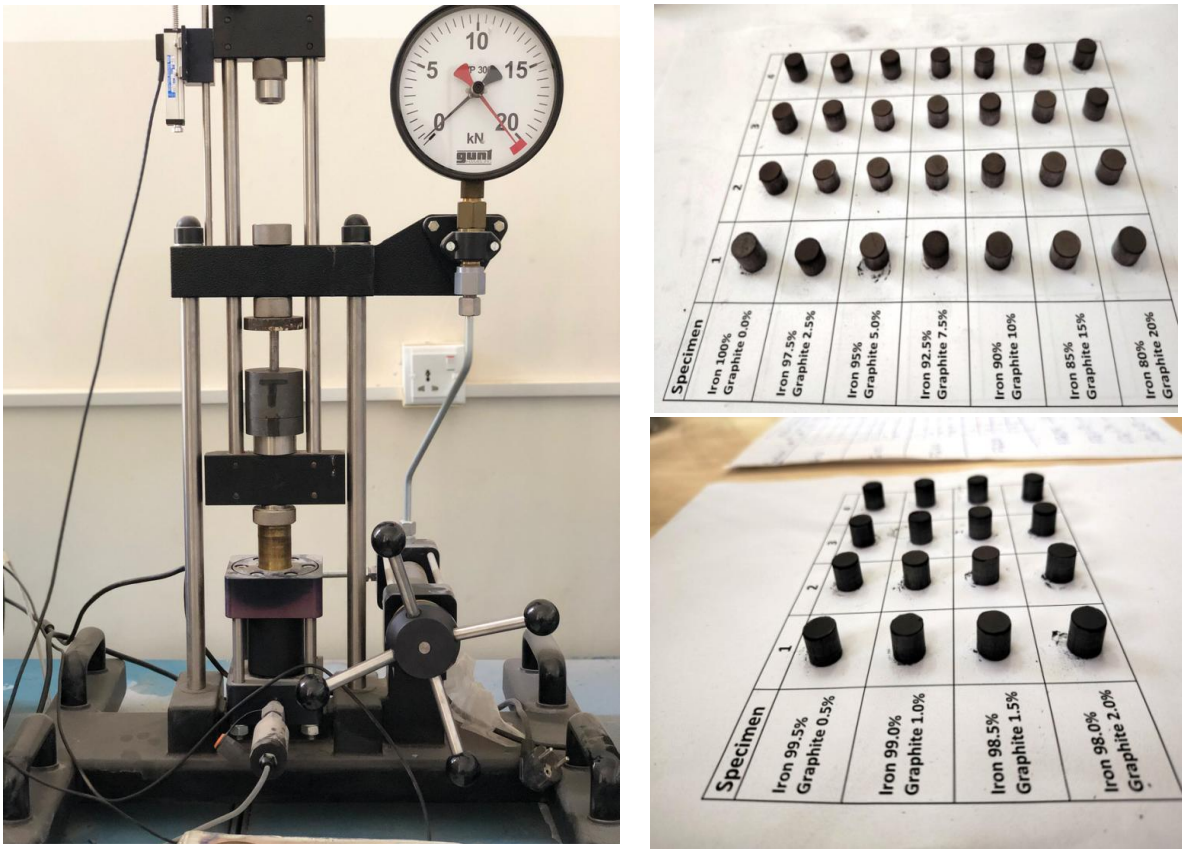


(a) (b)

**Fig 4.** (a) GUNT WP 300 universal testing machine used for specimen compaction, with the fabricated die set, (b) Samples after compaction.

.

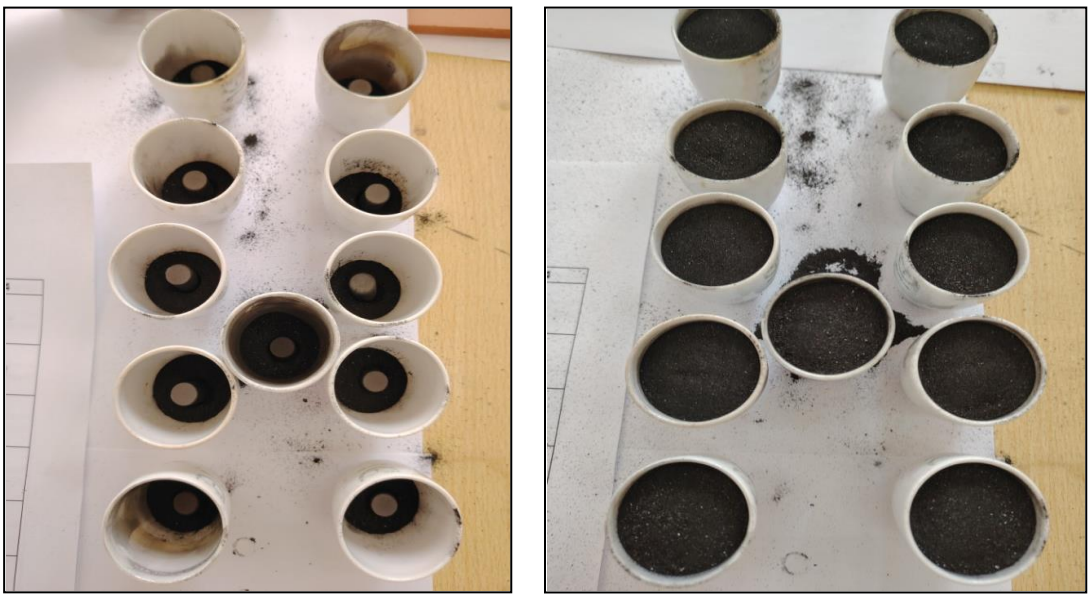

(a) (b)

**Fig 5.** Preparation of specimens for sintering: (a) specimens placed on a layer of anthracite inside the ceramic crucibles; (b) specimens fully covered with anthracite powder.

The specimens were designated as follows: F for pure sponge iron, G for graphite only, and FG-x for iron–graphite composites containing x wt% graphite. These designations are used consistently throughout the following sections.

### *2.4 Samples Testing*

A series of laboratory tests were conducted to evaluate the key physical and mechanical properties of the produced iron–graphite composites in accordance with relevant ASTM standards. Specimens containing more than 5 wt% graphite were excluded from the tests due to partial or complete separation of graphite during sintering.

#### *2.4.1 Green Strength*

The green strength, representing the ability of the unsintered compact to withstand handling and processing stresses, was determined using axial compression tests in accordance with ASTM E9 [16]. Tests were performed on one green specimen per composition using the GUNT WP 300 universal testing machine. The maximum load sustained before failure was recorded and converted to stress (MPa) based on the sample's cross-sectional area.

#### *2.4.2 Density and Porosity*

Green and sintered densities were measured following ASTM B962 [17] using the Archimedes' principle (buoyancy method). For green specimens, the density was calculated geometrically based on measured dimensions and weight. Porosity (φ) was estimated from the measured and theoretical densities of iron (7.87 g/cm³) and graphite (2.26 g/cm³) [18, 19]. Each reported value represents the average of at least three specimens.

#### *2.4.3 Dimensional Change*

Axial and volumetric dimensional changes after sintering were determined from the average pre- and post-sintering measurements using a vernier caliper (±0.01 mm). Results were expressed as percentage shrinkage (positive) or expansion (negative).

#### *2.4.4. Hardness*

Rockwell B hardness measurements were performed using a Shimadzu Rockwell Hardness Tester following ASTM E18 [20]. A 1/16 in (1.588 mm) steel ball indenter was used under a total load of 100 kgf. At least five readings were taken on each specimen surface, and the average ± standard deviation was reported as the hardness value (HRB).

#### *2.4.5 Abrasive Wear Test*

A two-body abrasive wear test was carried out using a custom-built pin-on-disc apparatus [21], following the ASTM G99 standard [22]. Tests were performed under dry sliding conditions at 23 °C and 50 % relative humidity, using a 5 N normal load, a 300 m sliding distance, and a disc speed of 100 rpm. The weight loss (ΔW) of each specimen was measured using a precision balance (± 0.1 mg), and the corresponding wear resistance (R) was calculated based on the measured density and standard relations

#### *2.4.6 Compressive Strength*

The compressive strength test was performed to assess the axial load-bearing capability of the sintered composites. Specimen dimensions were precisely measured with a digital vernier caliper (±0.01 mm). Testing was conducted using the GUNT WP 300 universal testing machine according to ASTM E9 [16]. Since the specimens did not fail under the applied load, the compressive strength was estimated from the hardness values, as discussed later.

#### *2.4.7 Microscopic Examination*

Microstructural characterization was performed following ASTM E3 [23], ASTM A247 [24], and EPMA guidelines [6], as well as Struers recommendations for powder metallurgy specimens [25]. Samples were hot-mounted using a Struers press, ground sequentially with SiC papers (120–1000 grit) under continuous

water flow, and polished with an alumina suspension. The microstructure was revealed by 2% Nital etching for 30 s. Optical images were obtained using a Leica DM2500 microscope, and ImageJ software was used to analyze porosity and graphite distribution within the matrix.

## 3. RESULTS AND DISCUSSION

### *3.1 Green Strength*

Green strength reflects the mechanical integrity of unsintered compacts and their ability to withstand handling stresses prior to sintering. It is mainly affected by particle size, morphology, compaction pressure, and graphite content [5, 26].

As shown in Figure 6, the addition of small amounts of graphite (≤ 2 wt%) slightly enhanced the green strength, which increased from 10.8 MPa for pure iron to an average of 12.25 MPa (≈ 13% improvement). This enhancement is attributed to the lubricating effect of graphite, which reduces interparticle friction and facilitates better particle rearrangement during compaction.

At higher graphite contents (> 2 wt%), a noticeable decline occurred, reaching 4.5 MPa at 2.5 wt% and only 1.5 MPa for pure graphite. This reduction results from the weak bonding and poor mechanical interlocking caused by excessive soft carbon phases [5, 7]. Therefore, the optimum graphite content for maintaining adequate green strength lies between 1 and 2 wt%.

### *3.2 Density and Porosity*

Density is one of the most fundamental physical indicators of powder consolidation quality, directly reflecting packing efficiency and interparticle bonding, while porosity inversely represents the fraction of unfilled voids within the structure. Green density provides an early indication of powder packing and compaction efficiency, whereas sintered density reflects the degree of metallurgical bonding achieved during sintering [3, 27].

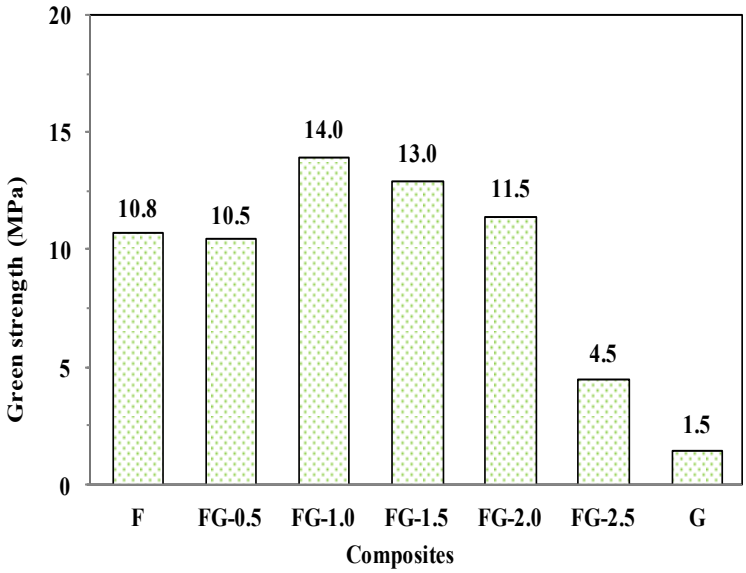


**Fig 6.** Green strength of the studied specimens.

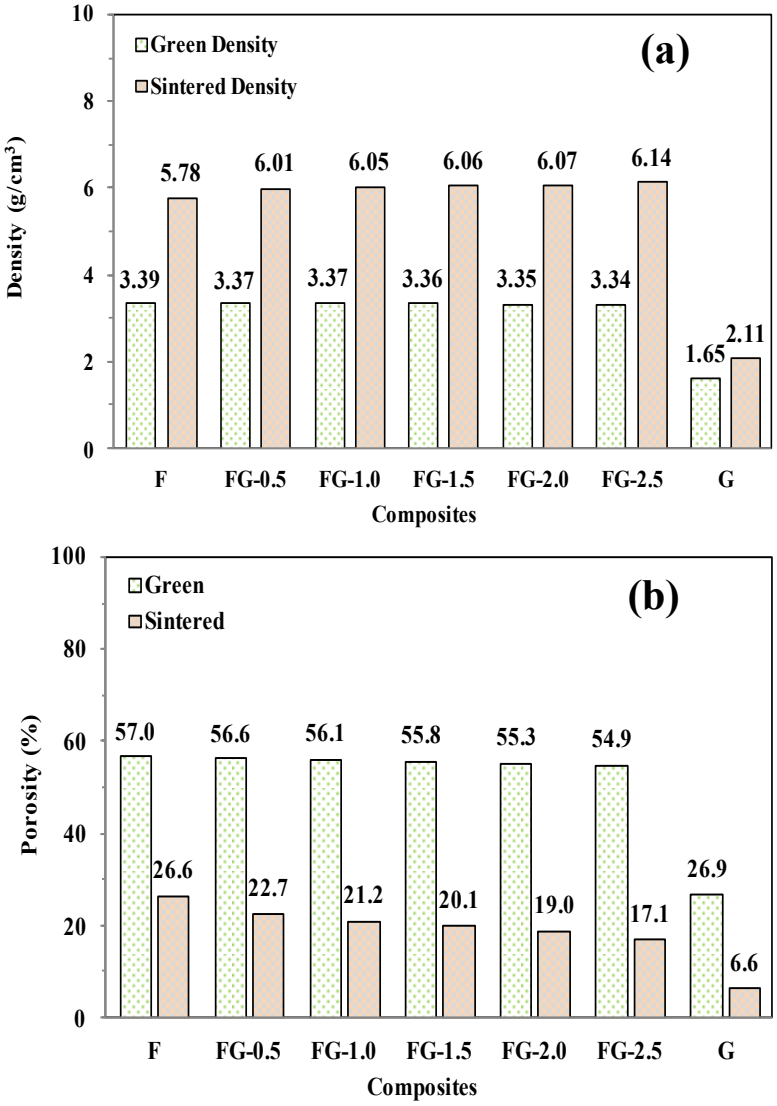


**Fig 7.** (a) Green and sintered densities of the specimens, (b) porosity of specimens in green and sintered states.

As illustrated in Figure 7(a), the green density of the specimens decreased slightly from 3.39 g/cm³ for pure iron to 3.34 g/cm³ for the FG-2.5 composition, while the graphite specimen exhibited the lowest value (1.65 g/cm³). The marginal decrease at low graphite levels (≤ 2.5 wt%) indicates that fine graphite particles did not significantly hinder the packing of iron powder.

After sintering, a pronounced densification occurred; the sintered density increased to 5.78 g/cm³ for pure iron and reached about 6.0–6.1 g/cm³ for composites containing up to 2.5 wt% graphite, corresponding to an average increase of approximately 79% over the green density. This improvement confirms the effectiveness of sintering in enhancing interparticle diffusion and bonding [3].

The evolution of porosity, shown in Figure 7(b), further supports this observation. The green porosity ranged from approximately 57% for pure Fe to 55% for FG-2.5, while post-sintering porosity markedly decreased to about 17–27%, corresponding to an average reduction of nearly 63%. This substantial decrease is primarily attributed to pore coalescence and shrinkage driven by surface energy minimization during the sintering process.

Overall, the pronounced reduction in porosity confirms improved particle bonding and microstructural consolidation, forming a solid basis for the enhanced mechanical performance discussed in the subsequent sections.

### *3.3 Dimensional Changes*

Dimensional changes are among the most characteristic phenomena accompanying the transition from the green to the sintered state in powder metallurgy compacts. These changes, whether shrinkage or expansion, directly affect the dimensional accuracy of the final product and must therefore be considered during die design. The extent of dimensional variation depends on several factors, including the green density, material composition, and sintering temperature, all of which must be optimized to achieve the desired mechanical and geometric properties.

Figure 8 shows representative compacts before and after sintering, including those with higher graphite contents (> 2.5 wt%). As seen in Figure 8(a), all Fe-based and Fe–graphite specimens exhibited noticeable shrinkage after sintering, whereas the graphite specimen displayed a distinct expansion. Figure 8(b) highlights the deterioration of specimens containing excessive graphite, showing visible deformation at 5–7.5 wt% and complete interfacial separation between graphite and the iron matrix at ≥ 10 wt%. This degradation is attributed to the nonuniform distribution of graphite at higher concentrations, which weakens interparticle bonding and promotes mechanical failure.

The relative dimensional changes in diameter and height are presented in Figure 9(a). The average shrinkage in the radial direction was about 18.4%, while the axial direction exhibited 18.1%. This contraction is primarily due to pore elimination and particle coalescence during sintering. Although these values may appear relatively high, they are consistent with the moderate compaction pressure used in this work (250 MPa). The close agreement between radial and axial shrinkage indicates a uniform green density distribution, which is advantageous for die design and dimensional predictability of the final product.

The volumetric shrinkage values, illustrated in Figure 9(b), averaged approximately 45.5%. This relatively high value reflects the initially low green density resulting from the moderate compaction pressure, which led to significant pore closure during sintering.

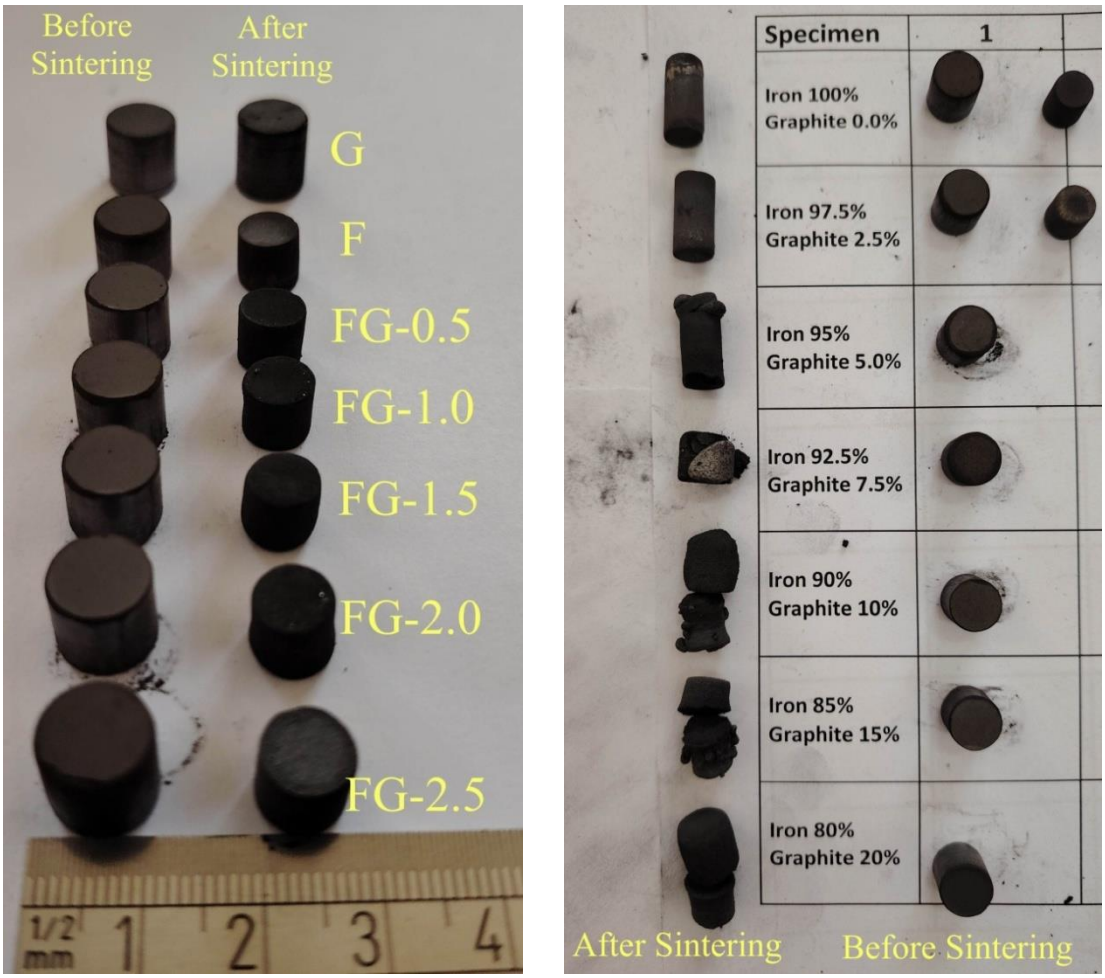


**Fig 8.** (a) Studied specimens before and after sintering, and (b) rejected specimens showing defects at high graphite contents.

As shown in Figure 9, the graphite specimen exhibited opposite behavior, with axial, radial, and volumetric expansions of about 6.9%, 2.9%, and 13.2%, respectively. These negative shrinkage values stem from the layered crystalline structure of graphite, which allows internal slippage during heating. Furthermore, the absence of true sintering neck formation between graphite particles prevents densification, allowing the structure to expand thermally instead of contracting [1, 3]. This expansion tendency likely contributed to the cracking and disintegration observed in composites with higher graphite contents, as noted earlier.

### *3.4 Hardness*

Hardness is a key indicator of the mechanical integrity of powder metallurgy composites, especially for self-lubricating materials subjected to frictional loading. As shown in Figure 10, the addition of small graphite fractions (0.5–2 wt%) significantly enhanced hardness compared with pure iron (77 HRB). The average hardness within this range reached about 95 HRB, with FG-0.5 exhibiting the highest value (97 HRB). This improvement is attributed to better particle bonding and densification during sintering, where graphite contributes to filling microvoids and stabilizing the load distribution.

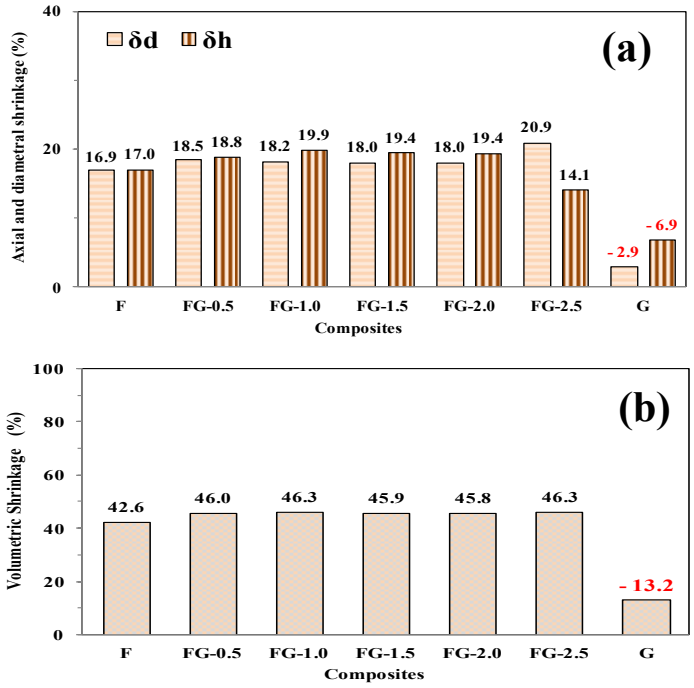


**Fig 9.** (a) Percentage change in height (δh) and diameter (δd) after sintering, (b) volumetric shrinkage percentage of the sintered specimens.

At higher graphite contents (≥ 2.5 wt%), hardness decreased to 68 HRB, likely due to graphite agglomeration and reduced matrix cohesion. The relatively high standard deviation for these samples also reflects non-uniform dispersion and local porosity variations.

These findings indicate that an optimal graphite range of 0.5–2 wt% achieves a favorable balance between self-lubrication and mechanical strength.

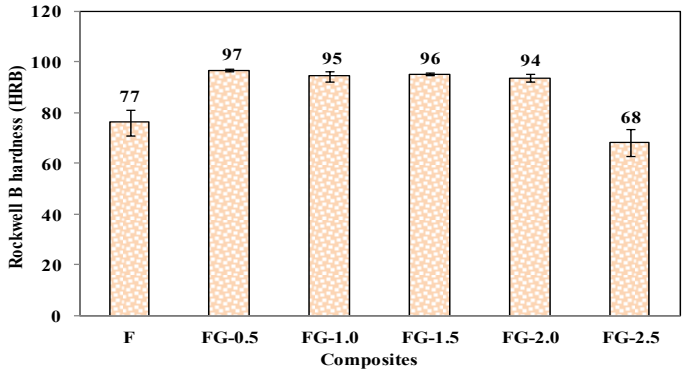


**Fig 10.** Rockwell hardness (HRB) of the studied specimens.

### *3.5 Abrasive Wear Behavior*

Abrasive wear resistance is a key performance criterion for self-lubricating materials, particularly in sliding components such as bearings and mechanical couplings. The incorporation of graphite enhances this property by forming a solid lubricating film that

minimizes direct metal-to-abrasive contact and material detachment.

Figure 11 presents the variation in weight loss (ΔW) and wear resistance (R) for the tested specimens. A significant reduction in weight loss was observed with graphite addition compared to pure sponge iron (F). Composites containing up to 2.5 wt% graphite exhibited an average reduction of about 74 % relative to the base material, with FG-1.0 showing the best performance - an ≈ 84 % reduction. This improvement is attributed to the lubricating action of graphite, which reduces frictional interaction and surface wear.

Conversely, wear resistance increased substantially with graphite addition, reaching its peak for FG-1.0 (≈ $2.4 \times 10^{11}$ m/m³), nearly six times higher than that of pure iron. At higher graphite contents (> 2 wt %), R slightly decreased, likely due to graphite agglomeration and weakened interparticle bonding within the metallic matrix.

The observed mechanism is visually supported in Figure 12, which shows a gray circular trace formed on the abrasive paper during testing. This trace confirms the development of a thin solid lubricating film of graphite during sliding, effectively reducing metal-to-metal contact and explaining the enhanced wear performance of the composites

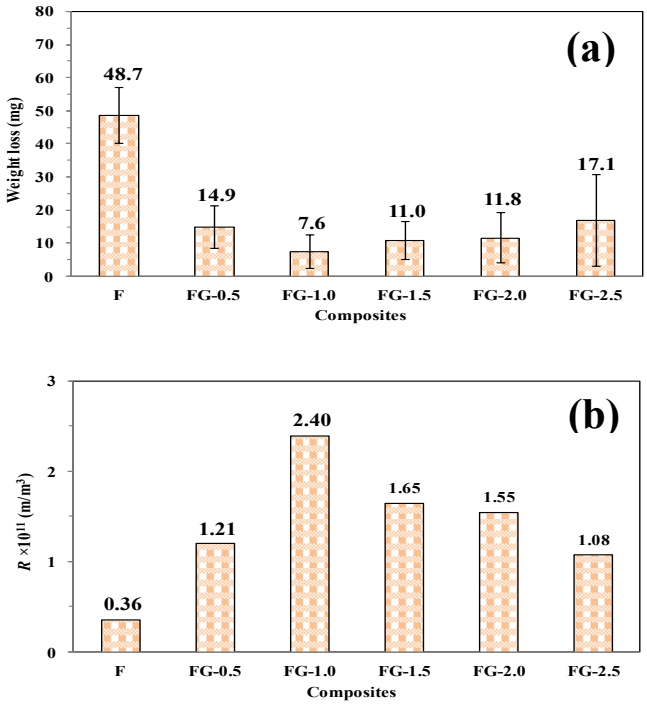


**Fig 11.** (a) Weight loss (ΔW) and (b) wear resistance (R) of the tested specimens.

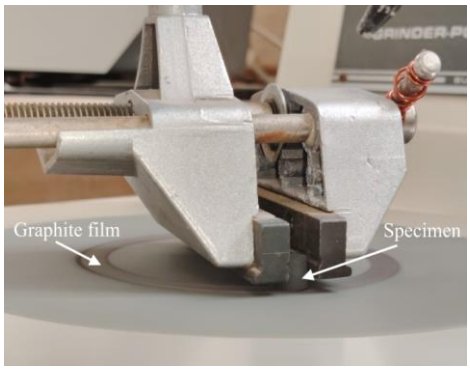


**Fig 12.** Specimen during the pin-on-disc wear test.

### *3.6 Compressive Strength*

The compressive strength test evaluates the ability of self-lubricating materials to withstand compressive loads without failure, which is critical for bearings and sliding components. This property is particularly sensitive to porosity and graphite distribution in powder metallurgy products.

Figure 13(a) shows the stress–strain curve of one of the tested specimens, which reached about 350 MPa without fracture, as illustrated in Figure 13(b). This trend was consistent across all specimens, where the curve termination coincided with the maximum load capacity of the testing machine (20 kN).

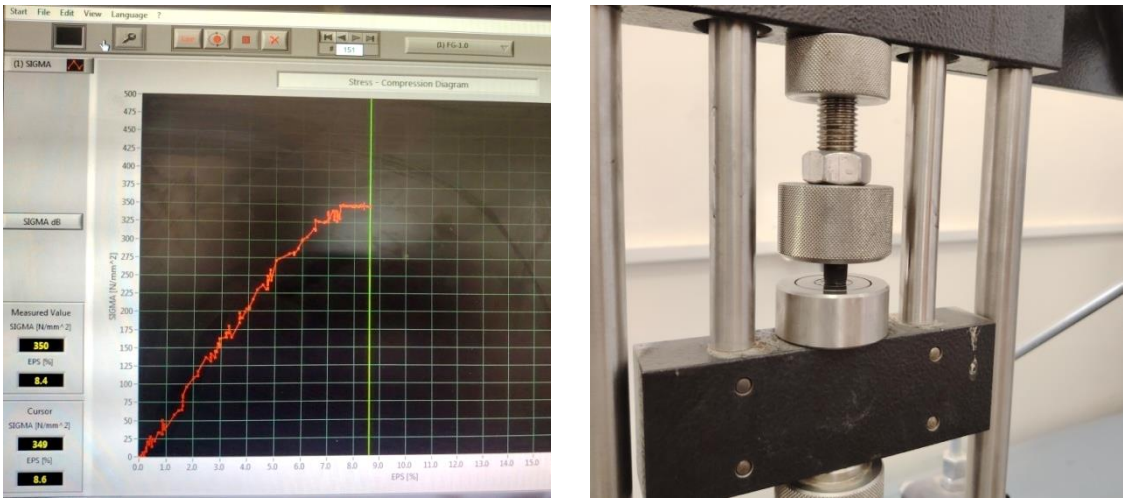


(a) (b)

**Fig 13. (**a) Stress–strain curve of a representative specimen, and (b) specimen during testing at maximum load.

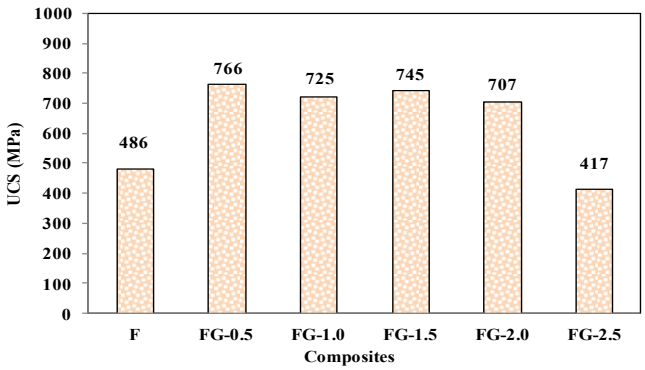


**Fig 14.** Calculated compressive strength of the tested specimens.

Because no specimen failed, the ultimate compressive strength (UCS) was estimated indirectly by converting Rockwell B hardness values to Brinell hardness (HB) using ASTM E140 [28], and applying the relation UCS = 3.45 × HB [29].

As illustrated in Figure 14, samples containing 0.5–2 wt% graphite showed improved UCS compared with pure iron (F), due to enhanced particle bonding and uniform graphite dispersion. The FG-2.5 specimen, however, exhibited lower strength, attributed to graphite agglomeration and localized porosity. These results align with the hardness and wear findings, confirming the consistent mechanical behavior of the composites.

### *3.7 Microstructural Examination*

Microstructural analysis is essential for interpreting the relationship between structure and properties in powder metallurgy (PM) materials. For self-lubricating composites, it provides insight into the uniformity of graphite dispersion within the iron matrix and its influence on porosity and mechanical behavior.

Representative micrographs of all specimens before etching at 50× magnification are shown in Figure 15. The pure iron sample (F) exhibits a relatively dense ferritic-pearlitic matrix with irregular dark pores - typical of PM compacts where complete densification is not achieved. In FG-0.5, small dark regions appear, corresponding to both fine pores and graphite inclusions. With increasing graphite content (up to 2.5 wt%), these regions grow larger and more numerous, indicating the progressive accumulation of graphite within the pores.

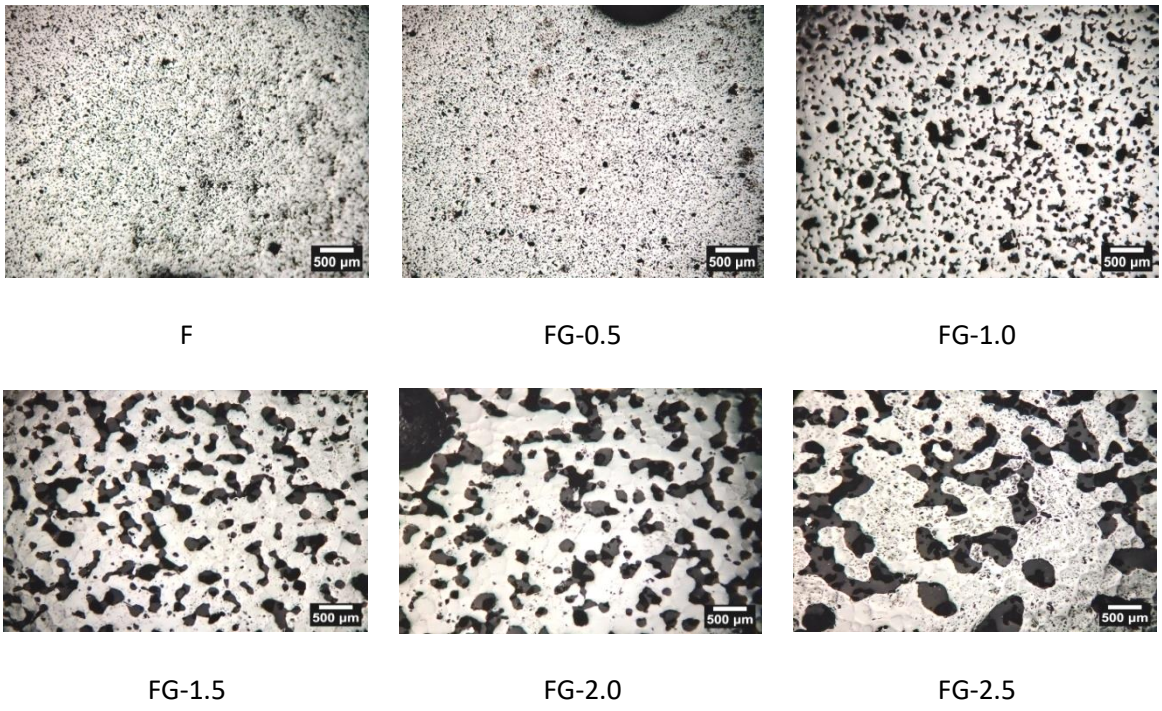


**Fig 15.** Optical micrographs of the investigated specimens before etching (50×).

After etching (Figure 16), metallic and non-metallic phases became more distinct. The FG-2.5 microstructure (Figure 17) shows coarse, irregular graphite clusters embedded in a ferrite–pearlite matrix with localized porosity. A blurred region (indicated by an arrow) was also observed, possibly representing cementite or ferrite boundaries; however, its precise identification would require SEM/EDS analysis. Such morphology explains the mechanical degradation observed at high graphite levels.

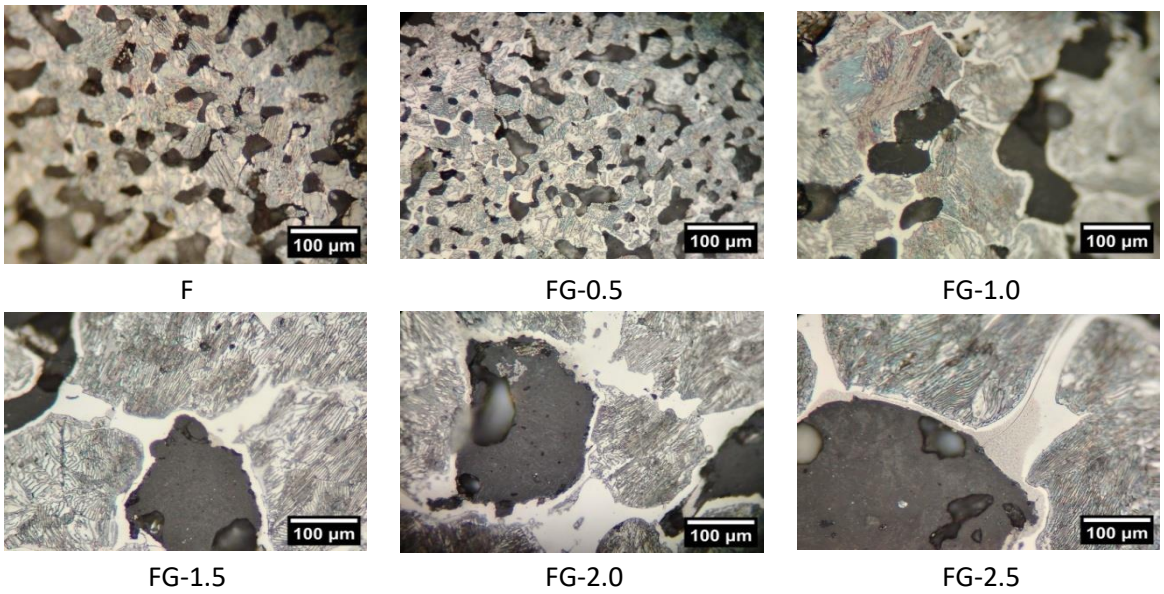


**Fig 16.** Optical micrographs of the etched specimens (500×).

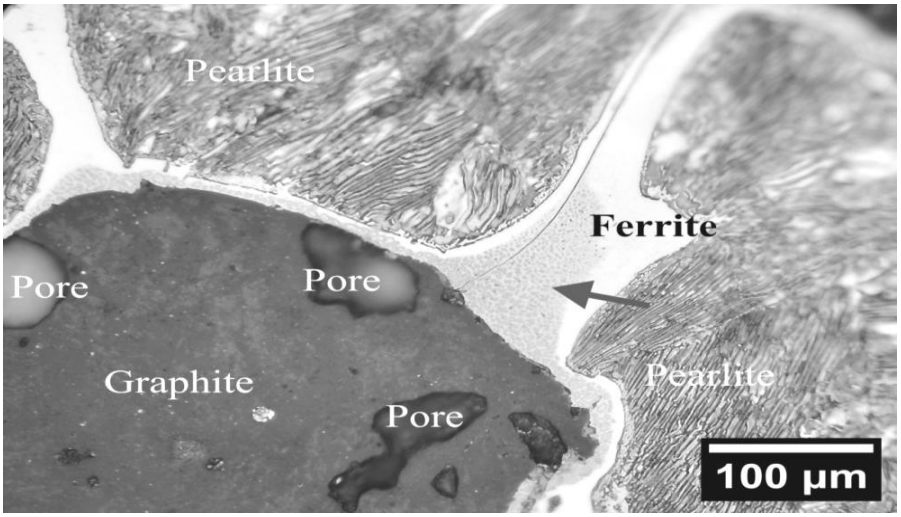


**Fig 17.** Microstructure of FG-2.5 showing graphite clusters and pores (500×).

To better illustrate the correlation between structure and performance, Figure 18 compares three representative samples: F, FG-1.0, and FG-2.5. The pure iron matrix shows uniformly distributed pores (~50 µm). FG-1.0 reveals homogeneously dispersed graphite particles (100–150 µm) surrounded by a well-bonded iron matrix, resulting in reduced porosity and enhanced cohesion - consistent with its superior hardness and wear resistance. In contrast, FG-2.5 exhibits elongated graphite agglomerates up to 2 mm in length and large voids (> 400 µm), covering nearly 40 % of the field area. This heterogeneous structure and weakened metallic continuity account for the reduced compressive strength and wear resistance previously discussed.

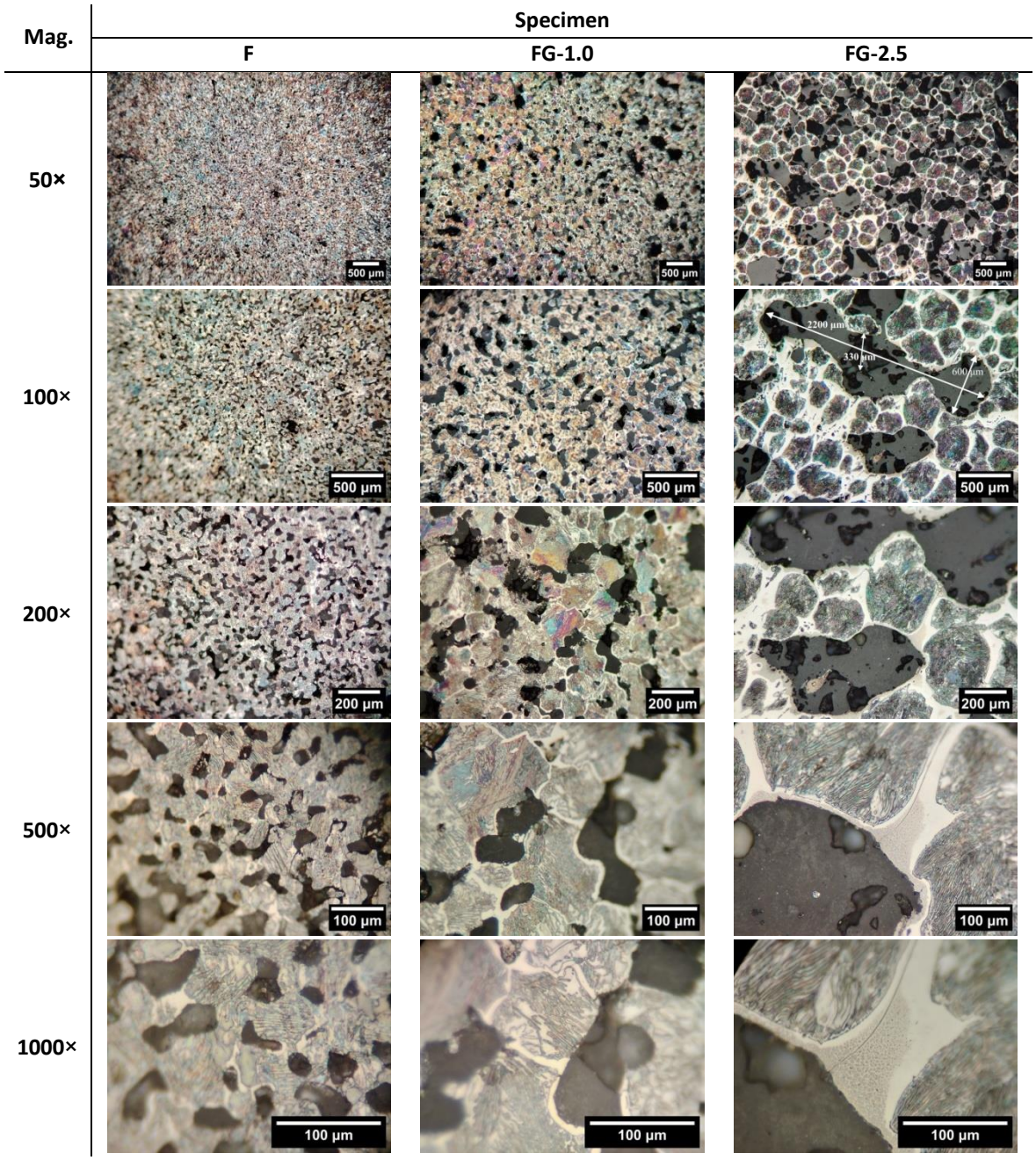


**Fig 18.** Comparative micrographs of F, FG-1.0, and FG-2.5 at different magnifications

## 4. CONCLUSIONS

In this study, self-lubricating iron-based composites reinforced with varying graphite contents were successfully fabricated using powder metallurgy, and their physical and mechanical properties were systematically evaluated. The addition of graphite caused only minor changes in both green and sintered densities, while sintering increased density by about 79% and reduced porosity by 63%, confirming the effectiveness of the process. Composites containing ≤ 2 wt% graphite exhibited adequate green strength (≈ 10.7 MPa) and enhanced hardness - about 24% higher than pure iron (average 95 HRB) -making them suitable for light to medium wear applications. Abrasive wear performance improved markedly, with an average weight loss reduction of 74% and a wear resistance increase exceeding 340%, reaching 570% for FG-1.0. Microstructural analysis supported these findings, showing a uniform graphite distribution and fine porosity that improved bonding and load transfer, whereas higher graphite contents (≥ 2.5 wt%) led to agglomeration and mechanical degradation. Overall, a graphite content near 1 wt% provides the best balance between strength, hardness, and self-lubricating performance. These findings demonstrate the industrial potential and cost-effectiveness of producing durable self-lubricating iron composites via conventional powder metallurgy. Future studies should explore intermediate graphite levels, the influence of particle size, higher compaction pressures, and controlled sintering atmospheres to further optimize performance and structural integrity.

## REFERNCES


[1] ASM International. *Powder Metal Technologies and Applications.* Vol. 7 of ASM Handbook. Novelty (OH): ASM International; 1998.

[2] German RM. *Powder Metallurgy Science.* Metal Powder Industries Federation; 1994.

[3] German RM. *Powder Metallurgy and Particulate Materials Processing: The Processes, Materials, Products, Properties, and Applications.* 2005.

[4] European Powder Metallurgy Association. *Introduction to Powder Metallurgy: The Process and Its Products.* 2008.

[5] Upadhyaya GS. *Powder Metallurgy Technology.* Cambridge: Int Science Publishing; 1997.

[6] European Powder Metallurgy Association. *Introduction to Metal Injection Moulding Technology: A Manufacturing Process for Precision Engineering Components.* Shrewsbury (UK): EPMA.

[7] Pierson HO. *Handbook of Carbon, Graphite, Diamond and Fullerenes: Properties, Processing and Applications.* Park Ridge (NJ): Noyes Publications; 1993.

[8] Sanyal A, et al. Study of graphite content and sintering temperature on wear and microstructure of Fe+C powder metallurgy preform. 2014.

[9] Zhang X, et al. Effects of graphite content and temperature on microstructure and mechanical properties of iron-based powder metallurgy parts. *J Mater Sci Res.* 2012;1:48.

[10] De Lima GA, et al. Controlling the solid-state reaction in Fe-$MoS_2$ self-lubricating composites for optimized tribological properties. *Lubricants.* 2022;10:142.

[11] Xiao J, et al. Friction of metal-matrix self-lubricating composites: Relationships among lubricant content, lubricating film coverage, and friction coefficient. *Friction.* 2020;8:517–530.

[12] Ye W, et al. Recent advances in self-lubricating metal matrix nanocomposites reinforced by carbonous materials: A review. *Nano Mater Sci.* 2024;6:701–713.

[13] Moghadam AD, et al. Mechanical and tribological properties of self-lubricating metal matrix nanocomposites reinforced by carbon nanotubes (CNTs) and graphene – a review. *Compos Part B Eng.* 2015;77:402–420.

[14] Araya N, et al. The influence of solid lubricant reservoir's morpho-dimensional evolution on the sliding wear of sintered iron-based self-lubricant composites. *Wear.* 2025;206032.

[15] Sari MO. Effect of graphite content on the physical and mechanical properties of self-lubricating iron-based composites manufactured by powder metallurgy [Bachelor's Graduation Project]. Misurata (Libya): Department of Materials Science and Engineering, Faculty of Engineering, Misurata University; 2025.

[16] ASTM International. *ASTM E9-09: Standard Test Methods of Compression Testing of*

*Metallic Materials at Room Temperature*. West Conshohocken (PA): ASTM International; 2009.

[17] ASTM International. *ASTM B962-15: Standard Test Methods for Density of Compacted or Sintered Powder Metallurgy (PM) Products Using Archimedes' Principle.* West Conshohocken (PA): ASTM International; 2015.

[18] CRC Press. *CRC Handbook of Chemistry and Physics.* Boca Raton (FL): CRC Press; 2004.

[19] Davis JR, editor. *Metals Handbook Desk Edition.* Novelty (OH): ASM International; 1998.

[20] ASTM International. *ASTM E18-20: Standard Test Methods for Rockwell Hardness of Metallic Materials.* West Conshohocken (PA): ASTM International; 2020.

[21] Ballem MA, et al. Effect of kaolin and phonolite particulates addition on hardness and abrasive wear behavior of glass-fiber composites. *Int J Eng Inf Technol (IJEIT).* 2025;13:54–61.

[22] ASTM International. *ASTM G99-17: Standard Test Method for Wear Testing with a Pin-on-Disk Apparatus.* West Conshohocken (PA): ASTM International; 2017.

[23] ASTM International. *ASTM E3-11 (Reapproved 2017): Standard Guide for Preparation of Metallographic Specimens.* West Conshohocken (PA): ASTM International; 2011.

[24] ASTM International. *ASTM A247-06: Standard Test Method for Evaluating the Microstructure of Graphite in Iron Castings.* West Conshohocken (PA): ASTM International; 2006.

[25] Struers ApS. *Metallographic Preparation of Powder Metallurgy Parts.* 2001.

[26] European Powder Metallurgy Association. *Introduction to Press and Sinter Technology: A Guide for Designers and Engineers.* Shrewsbury (UK): EPMA.

[27] European Powder Metallurgy Association. *Powder Metallurgy: The Process and Its Products.* Shrewsbury (UK): EPMA.

[28] ASTM International. *ASTM E140-07: Standard Hardness Conversion Tables for Metals.* West Conshohocken (PA): ASTM International; 2007.

[29] Callister WD, Rethwisch DG. *Materials Science and Engineering: An Introduction.* 9th ed. New York (NY): Wiley; 2013.